Article:
Chen, Yequan, Chen, Zhendong, Sun, Wenxuan et al. (9 more authors) (2022) Observation of an anisotropic ultrafast spin relaxation process in large-area WTe2films. Journal of Applied Physics. 163903. ISSN 1089-7550

https://doi.org/10.1063/5.0090935

Observation of an anisotropic ultrafast spin relaxation process in large-area WTe_2 films

Yequan Chen,[1,a)] Zhendong Chen,[1,a)] Wenxuan Sun,[1] Yongda Chen,[1] Xianyang Lu,[1] Xuezhong Ruan,[1] Fengqiu Wang,[1] Jing Wu,[2] Liang He,[1] Rong Zhang,[1] Yongbing Xu,[1,2,b)] and Xuefeng Wang[1,b)]

[1]Jiangsu Provincial Key Laboratory of Advanced Photonic and Electronic Materials, School of Electronic Science and Engineering, Collaborative Innovation Center of Advanced Microstructures, Nanjing University, Nanjing 210093, China

[2]York-Nanjing Joint Center in Spintronics, Department of Electronic Engineering and Department of Physics, The University of York, York YO10 5DD, United Kingdom

ABSTRACT

Weyl semimetal *Td*-WTe_2 hosts the natural broken inversion symmetry and strong spin-orbit coupling, which contains profound spin-related physics within a picosecond timescale. However, the comprehensive understanding of ultrafast spin behaviors in WTe_2 is lacking due to its limited quality of large-scale films. Here we report on an anisotropic ultrafast spin dynamics in highly-oriented *Td*-WTe_2 films using a femtosecond pump-probe technique at room temperature. A transient spin polarization-flip transition as fast as 0.8 ps is observed upon photoexcitation. The inversed spin is subsequently scattered by defects with duration of about 5.9 ps. The whole relaxation process exhibits an intriguing dual anisotropy of six-fold and two-fold symmetries, which stems from the energy band anisotropy of the WTe_2 crystalline structure and the matrix element effect, respectively. Our work enriches the insights into the ultrafast opto-spintronics in topological Weyl semimetals.

[a)]These authors contributed equally to this work.

[b)]Authors to whom correspondence should be addressed: ybxu@nju.edu.cn and xfwang@nju.edu.cn

I. INTRODUCTION

Topological Weyl semimetals have gained the growing interest owing to their remarkably exotic physics for potential applications.[1-4] Specifically, a representative Weyl topological semimetal,[5-7] WTe_2, has a unique band structure, enabling a rich spectrum of alluring properties, including extremely large non-saturating magnetoresistance,[8] pressure-/gate-tunable superconductivity,[9,10] quantum spin Hall effect,[11] nonlinear Hall effect,[12-14] large nonlinear optical properties[15-17] and notable spin-charge conversion properties.[18-20] Integration into the next-generation electronic/spintronic devices,[21-24] the ultrafast dynamics of low-dimension materials, e.g. graphene and topological insulators,[25-27] has attracted considerable attention.[28,29] However, the ultrafast research of *Td*-WTe_2 with naturally broken symmetry still remains very limited.[30-32] Thus, it becomes the urgent priority to uncover the nonequilibrium charge/spin dynamics of WTe_2 within a picosecond timescale. In an early report, Dai *et al*. revealed the ultrafast carrier dynamics of phonon-related thermalization and recombination process in the bulk WTe_2.[33] Then, Wang *et al*. observed the ultrafast spin dynamics in the polycrystalline WTe_2 films.[34] Till now, however, the full understanding of spin dynamics in WTe_2 is elusive due to the bad quality of large-scale films, which limits its practical applications in spintronics.

The band distribution and orbital structure play important roles in the ultrafast spin dynamics. This usually results in the intriguing anisotropic characteristic, which has been shown in van der Waals heterostructures (e.g.,

WS_2/graphene)[35] and manganite oxides (e.g., $La_{0.7}Sr_{0.3}MnO_3/SrTiO_3$)[36]. However, such an anisotropic spin relaxation process cannot be found in topological insulators due to almost isotropic band structures close to Fermi level around Γ point in the momentum space.[37,38] In this regard, WTe_2 exceptionally hosts the broken inversion symmetry with the naturally anisotropic band structure, enabling the observation of the interesting anisotropic spin dynamics. Its exotic band inversion and anticrossings with spin splitting at the Fermi level have been predicted by the first-principles calculations.[39,40]

In this work, we observe the ultrafast spin dynamics in highly-oriented and large-area orthorhombic (*Td*) phase of WTe_2 films by time-resolved magneto-optical Kerr effect (TR-MOKE) technique at room temperature. After the photoexcitation by circular polarized pump light, the whole spin relaxation experiences two processes, i.e., a transient spin polarization-flip intra-band transition with a lifetime of 0.8 ps and a subsequent defect scattering process with a lifetime of 5.9 ps. Notably, a dual anisotropy, i.e., six-fold and two-fold symmetries, is established by tuning the polarization orientation of the probe light. In contrast, these phenomena are absent in the polycrystalline films containing the abundant defects.

II. EXPERIMENTAL

A. Sample fabrication

The large-area, high-quality *Td*-WTe_2 films with the thickness of about 100

nm were fabricated on mica substrates by the pulsed laser deposition technique and post annealing, as described elsewhere.[41-43] WTe_2 has a layered structure with an additional lattice distortion along the crystallographic axis *b* of tungsten chain [see Fig. 1(a)]. Three 100-nm-thick WTe_2 films (named #1, #2, and #3, see the supplementary material for the detailed growth conditions) were fabricated. The structural characterization has confirmed the high quality of the WTe_2 thin films before the ultrafast measurement (Fig. S1, supplementary material). Unless the special statement, the sample described here denotes #1.

B. TR-MOKE and transient reflectivity measurements

The wavelength of 800 nm (1.51 eV) pulsed laser was generated in the Ti:sapphire regenerative amplifier (a repetition rate of 1 kHz, pulse duration of ~50 fs, and fluence of ~1 mJ/cm^2). In order to reduce the noise related to the stray pump light, the nondegenerate mode was used to measure the spin relaxation process. The pulsed laser subsequently went through a beam splitter. One beam of 90% power intensity was used as a pump beam. The other beam was frequency-doubled (400 nm, 3.02 eV) by a β-BaB_2O_4 (BBO) crystal, which was treated as a probe beam. The pump beam was varied to be circularly polarized via a combination of linear polarizer and a quarter-wave plate. The probe beam was ensured as a linear polarized light by a Glan-Taylor prism. The polarization plane was rotated by a half-wave plate set behind the Glan-Taylor prism. The pump beam was incident perpendicularly on the sample surface with a spot size of ~500 μm in diameter. The incident angle of the probe beam (spot size ~250

μm) is 4° with respect to the sample normal direction. The angle φ represents the rotation angle of the polarized direction of probe light with respect to the incident plane, while the angle α is defined as the azimuthal angle between the crystallographic axis [100] of the WTe_2 film and the spatial x axis. After reflection by the sample, the probe beam was analyzed by a series of half-wave plate, Wollaston beam splitter (WBS), and balanced photodetector (BPD). The time delay between two beams was controlled by a mechanical delay stage.

The transient reflectivity was carried out by the Ti:sapphire laser as well. The femtosecond laser beam with 800 nm was divided into a pump beam and a probe beam. Their spot diameters were 500 and 250 μm, respectively. Both pulses were focused onto the sample noncollinearly. The differential reflectivity dynamics was acquired as a function of the time delay between the cross-polarized pump and probe pulses.

III. RESULTS

The schematic setup of the TR-MOKE technique is shown in Fig. 1(b). After the circularly polarized light pump, the excitation of the electrons in WTe_2 obeys both the energy conservation and the angular momentum conservation: an electron in the valence band (VB) absorbs a photon and transfers to the conduction band (CB) with a change of ±1 in magnetic quantum number $\mathbf{m_j}$. Therefore, the excited electrons have instant net out-of-plane spin polarization according to the optical selection rules.[25,44,45] The Kerr rotation angle (θ_k) of the probe light is used to

describe the pump-induced spin polarization via the relationship of $\theta_k \sim M_p \cdot k$, where M_p represents equivalent magnetization resulted from the instant net out-of-plane spin polarization of excited electrons, and k is the wave vector.[46] In WTe_2, the time-resolved Kerr signal changes sign with the different helicity (σ^+ and σ^-) of the pump beam, indicating that a nonequilibrium net spin polarization is generated [Fig. 1(c)]. During the experiment, imperfectly balanced optical bridge can bring an artifact, i.e., helicity-independent partial signal of the transient reflectivity, which is mixed in the Kerr signal by σ^+ or σ^- pump. To rule out this spurious artifact, the difference of Kerr signals between σ^+ and σ^- [$\Delta\theta_k(\sigma^+) - \Delta\theta_k(\sigma^-)$] is carried out and applied as the net Kerr signal.[25,34] In addition, the fluence-dependent Kerr signals and transient reflectivity spectra are displayed in Fig. S2 (supplementary material), indicating the large excited electron density of states in the deep valence band of WTe_2 films.

The polarization orientation of the probe light [i.e., φ angle shown in Fig. 1(b)] is changed to detect the anisotropy of this spin relaxation. When $\varphi = 0^o$, the electric field of light lies in the plane of the incident probe beam, which is P-polarization (P-pol). And $\varphi = 90^o$ is S-polarization (S-pol). Note that the spin relaxation process displays the distinct φ dependence [Fig. 2(a)]. The spin relaxation is fitted by a biexponential decay model using the equation of $A_1 \cdot e^{-t/\tau_1} + A_2 \cdot e^{-t/\tau_2}$, where A_1 and A_2 denote the amplitudes; τ_1 and τ_2 represent the corresponding spin lifetime. The fitting results indicate that the whole spin relaxation process is composed of two sub-processes [Fig. 2(b)]. Figure 2(c)

shows the plot of φ dependence of fitted A_1 and A_2 amplitudes. Interestingly, both φ-dependent A_1 and A_2 curves show the distinct anisotropy, as expected. The signs of A_1 and A_2 are always opposite. The first sub-process experiences the spin polarization-flip transition with the lifetime τ_1 of ~0.8 ps. The second sub-process has the lifetime τ_2 of ~5.9 ps. Both of the sub-processes show the almost independence with the φ angle [Fig. 2(d)], indicating the isotropic relaxation rates (τ_1^{-1} and τ_2^{-1}).

Figure 3(a) shows the transient reflectivity spectrum of the WTe_2 films. The spectrum is also fitted by the biexponential decay model as shown above.[47] The lifetime of the electron-hole recombination process is fitted as ~72.2 ps, much longer than the spin lifetime τ_2 of 5.9 ps. Thus, the net spin almost vanishes before the recombination of the carriers. As a control experiment, the Kerr signals of samples with the different defect densities (#2 and #3) are shown in Fig. 3(b). Sample #2 contains a little more defect due to #1 oxidation in atmosphere. Sample #3 possesses abundant defects. The typical TR-MOKE setup condition is set at $\varphi = 10^o$. By the biexponential decay model fitting, the spin lifetimes of two sub-processes of Sample #2 are 0.8 and 3.6 ps, respectively. It is clear that more defects in the WTe_2 films only deteriorate the second sub-process (from the initial 5.9 to 3.6 ps). While the abundant defects contained in WTe_2 (Sample #3) completely suppress the spin-related signals [Fig. 3(b)]. Thus, the second sub-process with the lifetime τ_2 of ~5.9 ps is dominated by the defect scattering.

IV. DISCUSSION

To address the origin of the observed anisotropic ultrafast spin relaxation process in Fig. 2(c), the sine function is used to fit the φ-dependent A_1 and A_2 curves (Table S1, supplementary material). It demonstrates that the anisotropy consists of a six-fold and two-fold symmetries. Meantime, the a- crystallographic axis [shown in Fig. 1(a)] of WTe_2 films is rotated to explore the α-angle-dependent spin relaxation of WTe_2 films. The α-azimuthal angle is also shown in Fig. 1(b). Although the detected point on WTe_2 films changes when rotating the sample, it does not change the whole anisotropy of the spin relaxation process (Fig. S3, supplementary material). The α-dependent A_1 (A_2) only features a six-fold symmetry (~60°), as shown in Fig. 4(a), which exactly agrees with one of the symmetries deduced from Fig. 2(c). It is reasonable to attribute the six-fold symmetry to the lattice structure of WTe_2 films. Considering the monoclinic structure of WTe_2 and the hexagonal structure of mica substrate, there is a symmetry mismatch between the WTe_2 film and substrate. Hence, three energetically equivalent domains are suggested in WTe_2 films on mica.[48] These domains are rotated by 120° with each other, resulting in the six-fold symmetry of the spin relaxation in the WTe_2 films.

Though the φ-dependent two-fold symmetry unexpectedly vanishes in α-dependent TR-MOKE measurements, two-fold symmetry can be extracted from the data in Fig. 2(c) after subtraction of the six-fold symmetry (Fig. S4,

supplementary material). The maximum and minimum values (at 0° and 90°) of the two-fold symmetry are almost opposite to each other, indicating that P-pol and S-pol probe beam exactly detect the ultrafast spin relaxation with the opposite polarization direction. We notice that electrons in the different orbitals may be only detected by either P-pol or S-pol probe beam, which strictly obeys the rule of the matrix element effect.[48] In WTe_2, such a phenomenon has been unambiguously observed by the angle-resolved photoemission spectroscopic measurements.[49] Figure 4(b) schematically shows the Fermi surface mapping with electron pockets. The $\boldsymbol{d_{z^2}}$ orbital is located at the farther half-part of the electron pocket from the Γ point, while the $\boldsymbol{d_{xz}}$, $\boldsymbol{d_{yz}}$ and $\boldsymbol{p_y}$ orbitals lie at the other half-part. They can be only detected by P- or S-pol probe beams due to the matrix element effect.[50] More discussion can be found in Fig. S5 (supplementary material).

The band structure and the spin texture of WTe_2 have been explored in theory and experiment.[39,40,51] The band structure around the Fermi surface is hence discussed by Dirac Fermion model with strong spin-orbit coupling, where the spin-orbit coupling strength along x direction (v_x) is set as 0.2-0.4 eV·Å. Taking the $-k_x$ axis of Brillouin zone as an example, the schematic diagrams of the corresponding band structure and spin texture are shown in Fig. 4(c). The dotted rectangular box contains the energy levels of conduction band (CB) and valence band (VB), where the red and blue curves denote the spin up and spin down in CB, respectively. Due to the strong SOC, the bottom of the CB is split

into two sub-bands with the different spin orientation. The spin textures of the left-part and right-part branches in CB are inversed, which denotes the $\boldsymbol{d_{z^2}}$ orbital and $\boldsymbol{d_{xz}}$, $\boldsymbol{d_{yz}}$, $\boldsymbol{p_y}$ orbitals, respectively.[48] When the probe beam is adjusted to P-pol, we actually detect the spin relaxation in the left-part branch ($\boldsymbol{d_{z^2}}$ orbital) of CB. Upon the applied circularly polarized pump (1.51 eV), the electron with the net spin is firstly excited from the deep VB to the Position A. Secondly, it instantly decays to Position B via the intra-band particle's interaction. Such a process usually lasts about tens of femtoseconds, which escapes from our detection limit of TR-MOKE. Thirdly, the excited electron transits from Position B to C at the lower sub-band with the opposite spins, corresponding to the first spin-flip sub-process. This intra-band transition lasts about 0.8 ps, which is ascribed to the Elliott-Yafet mechanism[52] dominated by the electron-electron interaction.[53,54] Finally, the inversed spin experiences the second sub-process with the lifetime of about 5.9 ps. The similar spin relaxation is derived from the right-part branch ($\boldsymbol{d_{xz}}$, $\boldsymbol{d_{yz}}$ and $\boldsymbol{p_y}$ orbitals) of CB through S-pol probe. However, the direction of spin polarization in the right-part branch is opposite to that of the left-part branch. Consequently, the two-fold symmetry of the spin relaxation is attributed to the φ-dependent P- and S-pol components of the probe beam.

V. CONCLUSION

In summary, we have clarified the room-temperature ultrafast spin

dynamics by TR-MOKE technique in large-area, high-quality *Td*-WTe_2 films. The whole ultrafast spin relaxation process experiences the intra-band spin polarization-flip transition and the subsequent defect scattering process. Remarkably, six-fold and two-fold symmetries of the ultrafast spin relaxation process are observed by tuning the polarization orientation of the probe light. Such a dual anisotropy is attributed to the anisotropic band structure of WTe_2 and the matrix element effect, respectively. The WTe_2 may have the potential for future multi-channel spintronic devices in view of the intrinsic interaction between the spin and orbital. Furthermore, the strong sensitivity of the orbital upon the polarity of the probe light could offer an opportunity to develop the ultrafast optoelectronic devices.

SUPPLEMENYARY MATERIAL

See the supplementary material for the detailed information of samples, structural characterization, and the additional ultrafast dynamic results.

ACKNOWLEDGMENTS

We are grateful to F. Q. Song, C. F. Zhang, P. Wang, and B. Liu for fruitful discussions. This work was partially supported by the National Natural Science Foundation of China (Grant Nos. 61822403, 11874203, and 11774160), and the National Key R&D Program of China (Grant Nos. 2017YFA0206304 and 2016YFA0300803).

AUTHOR DECLARATIONS

Conflict of Interest

The authors declare no conflicts of interest.

DATA AVAILABILITY

The data that support the findings of this study are available from the corresponding author upon reasonable request.

REFERENCES

[1]S. M. Huang, S. Y. Xu, I. Belopolski, C. C. Lee, G. Chang, B. Wang, N. Alidoust, G. Bian, M. Neupane, C. Zhang, S. Jia, A. Bansil, H. Lin, and M. Z. Hasan, A Weyl Fermion semimetal with surface Fermi arcs in the transition metal monopnictide TaAs class, Nat. Commun. **6**, 7373 (2015).

[2]S.-Y. Xu, I. Belopolski, N. Alidoust, M. Neupane, G. Bian, C. Zhang, R. Sankar, G. Chang, Z. Yuan, C.-C. Lee, S.-M. Huang, H. Zheng, J. Ma, D. S. Sanchez, B. Wang, A. Bansil, F. Chou, P. P. Shibayev, H. Lin, S. Jia, and M. Z. Hasan, Discovery ofa Weyl fermion semimetal and topological Fermi arcs, Science **349**, 613 (2015).

[3]A. A. Soluyanov, D. Gresch, Z. Wang, Q. Wu, M. Troyer, X. Dai, and B. A. Bernevig, Type-II Weyl semimetals, Nature **527**, 495 (2015).

[4]X. Wan, A. M. Turner, A. Vishwanath, and S. Y. Savrasov, Topological semimetal and Fermi-arc surface states in the electronic structure of pyrochlore iridates, Phys. Rev. B **83**, 205101 (2011).

[5]X.-C. Pan, X. Wang, F. Song, and B. Wang, The study on quantum material WTe_2, Adv. Phys. X **3**, 593 (2018).

[6]J. Augustin, V. Eyert, T. Bo¨ker, W. Frentrup, H. Dwelk, C. Janowitz, and R. Manzke, Electronic band structure of the layered compound Td-WTe_2, Phys. Rev. B **62**, 10812 (2000).

[7]M. Cao, Z. Wang, L. Ma, L. Zhang, M. Wang, Y. Liu, J. He, and X. Xi, Tungsten Ditelluride: Synthesis, Structure, and Magnetoresistance Property, Adv. Electron. Mater. **7**, 2000893 (2021).

[8]M. N. Ali, J. Xiong, S. Flynn, J. Tao, Q. D. Gibson, L. M. Schoop, T. Liang, N. Haldolaarachchige, M. Hirschberger, N. P. Ong, and R. J. Cava, Large, non-saturating magnetoresistance in WTe_2, Nature **514**, 205 (2014).

[9]V. Fatemi, S. Wu, Y. Cao, L. Bretheau, Q. D. Gibson, K. Watanabe, T. Taniguchi, R. J. Cava, and P. Jarillo-Herrero, Electrically tunable low-density superconductivity in a monolayer topological insulator, Science **362**, 926 (2018).

[10]E. Sajadi, T. Palomaki, Z. Fei, W. Zhao, P. Bement, C. Olsen, S. Luescher, X. Xu, J. A. Folk, and D. H. Cobden, Gate-induced superconductivity in a monolayer topological insulator, Science **362**, 922 (2018).

[11]S. Wu, V. Fatemi, Q. D. Gibson, K. Watanabe, T. Taniguchi, R. J. Cava, and P. Jarillo-Herrero, Observation of the quantum spin Hall effect up to 100 kelvin in a monolayer crystal, Science **359**, 76 (2018).

[12]Q. Ma, S. Y. Xu, H. Shen, D. MacNeill, V. Fatemi, T. R. Chang, A. M. Mier Valdivia, S. Wu, Z. Du, C. H. Hsu, S. Fang, Q. D. Gibson, K. Watanabe, T. Taniguchi, R. J. Cava, E. Kaxiras, H. Z. Lu, H. Lin, L. Fu, N. Gedik, and P. Jarillo-Herrero, Observation of the nonlinear Hall effect under time-reversal-symmetric conditions, Nature **565**, 337 (2019).

[13]Z. He and H. Weng, Giant nonlinear Hall effect in twisted bilayer WTe_2, npj Quantum Mater. **6**, 101 (2021).

[14]A. Tiwari, F. Chen, S. Zhong, E. Drueke, J. Koo, A. Kaczmarek, C. Xiao, J. Gao, X. Luo, Q. Niu, Y. Sun, B. Yan, L. Zhao, and A. W. Tsen, Giant c-axis nonlinear anomalous Hall effect in Td-$MoTe_2$ and WTe_2, Nat. Commun. **12**, 2049 (2021).

[15]M. He, Y. Chen, L. Zhu, H. Wang, X. Wang, X. Xu, and Z. Ren, Third-order nonlinear optical properties of WTe_2 films synthesized by pulsed laser deposition, Photonics Res. **7**, 1493 (2019).

[16]W. Gao, L. Huang, J. Xu, Y. Chen, C. Zhu, Z. Nie, Y. Li, X. Wang, Z. Xie, S. Zhu, J. Xu, X. Wan, C. Zhang, Y. Xu, Y. Shi, and F. Wang, Broadband photocarrier dynamics and nonlinear absorption of PLD-grown WTe_2 semimetal films, Appl. Phys. Lett. **112**, 171112 (2018).

[17]E. Drueke, J. Yang, and L. Zhao, Observation of strong and anisotropic nonlinear optical effects through

polarization-resolved optical spectroscopy in the type-II Weyl semimetal Td−WTe_2, Phys. Rev. B **104**, 064304 (2021).

[18]X.-G. Ye, P.-F. Zhu, W.-Z. Xu, N. Shang, K. Liu, and Z.-M. Liao, Orbit-Transfer Torque Driven Field-Free Switching of Perpendicular Magnetization, Chin. Phys. Lett. **39**, 037303 (2022).

[19]Y. Fan, H. Li, M. Dc, T. Peterson, J. Held, P. Sahu, J. Chen, D. Zhang, A. Mkhoyan, and J.-P. Wang, Spin pumping and large field-like torque at room temperature in sputtered amorphous WTe_{2-x} films, APL Mater. **8**, 041102 (2020).

[20]Q. Xie, W. Lin, S. Sarkar, X. Shu, S. Chen, L. Liu, T. Zhao, C. Zhou, H. Wang, J. Zhou, S. Gradečak, and J. Chen, Field-free magnetization switching induced by the unconventional spin–orbit torque from WTe_2, APL Mater. **9**, 051114 (2021).

[21]I. Z˘utic´, J. Fabian, and S. D. Sarma, Spintronics: Fundamentals and applications, Rev. Mod. Phys. **76**, 323 (2004).

[22]M. W. Wu, J. H. Jiang, and M. Q. Weng, Spin dynamics in semiconductors, Phys. Rep. **439**, 61 (2010).

[23]M. Zhang, X. Wang, F. Song, and R. Zhang, Layered Topological Insulators and Semimetals for Magnetoresistance Type Sensors, Adv. Quantum Technol. **2**, 1800039 (2018).

[24]W. Zhuang, Z. Chen, and X. Wang, Large-area fabrication of 2D layered topological semimetal films and emerging applications, Adv. Phys.: X **7**, 2034529 (2022).

[25]M. C. Wang, S. Qiao, Z. Jiang, S. N. Luo, and J. Qi, Unraveling Photoinduced Spin Dynamics in the Topological Insulator Bi_2Se_3, Phys. Rev. Lett. **116**, 036601 (2016).

[26]V. Iyer, Y. P. Chen, and X. Xu, Ultrafast Surface State Spin-Carrier Dynamics in the Topological Insulator Bi_2Te_2Se, Phys. Rev. Lett. **121**, 026807 (2018).

[27]Y. D. Glinka, J. Li, T. He, and X. W. Sun, Clarifying Ultrafast Carrier Dynamics in Ultrathin Films of the Topological Insulator Bi_2Se_3 Using Transient Absorption Spectroscopy, ACS Photonics **8**, 1191 (2021).

[28]D. Pesin and A. H. MacDonald, Spintronics and pseudospintronics in graphene and topological insulators, Nat. Mater. **11**, 409 (2012).

[29]Y. Li, J. Shi, Y. Mi, X. Sui, H. Xu, and X. Liu, Ultrafast carrier dynamics in two-dimensional transition metal dichalcogenides, J. Mater. Chem. C **7**, 4304 (2019).

[30]M. Chen, K. Lee, J. Li, L. Cheng, Q. Wang, K. Cai, E. E. M. Chia, H. Chang, and H. Yang, Anisotropic Picosecond Spin-Photocurrent from Weyl Semimetal WTe_2, ACS Nano **14**, 3539 (2020).

[31]E. J. Sie, C. M. Nyby, C. D. Pemmaraju, S. J. Park, X. Shen, J. Yang, M. C. Hoffmann, B. K. Ofori-Okai, R. Li, A. H. Reid, S. Weathersby, E. Mannebach, N. Finney, D. Rhodes, D. Chenet, A. Antony, L. Balicas, J. Hone, T. P. Devereaux, T. F. Heinz, X. Wang, and A. M. Lindenberg, An ultrafast symmetry switch in a Weyl semimetal, Nature **565**, 61 (2019).

[32]P. Hein, S. Jauernik, H. Erk, L. Yang, Y. Qi, Y. Sun, C. Felser, and M. Bauer, Mode-resolved reciprocal space mapping of electron-phonon interaction in the Weyl semimetal candidate Td-WTe_2, Nat. Commun. **11**, 2613 (2020).

[33]Y. M. Dai, J. Bowlan, H. Li, H. Miao, S. F. Wu, W. D. Kong, P. Richard, Y. G. Shi, S. A. Trugman, J.-X. Zhu, H. Ding, A. J. Taylor, D. A. Yarotski, and R. P. Prasankumar, Ultrafast carrier dynamics in the large-magnetoresistance material WTe_2, Phys. Rev. B **92**, 161104 (2015).

[34]Q. Wang, J. Li, J. Besbas, C. H. Hsu, K. Cai, L. Yang, S. Cheng, Y. Wu, W. Zhang, K. Wang, T. R. Chang, H. Lin, H. Chang, and H. Yang, Room-Temperature Nanoseconds Spin Relaxation in WTe_2 and $MoTe_2$ Thin Films, Adv. Sci. **5**, 1700912 (2018).

[35]L. A. Benítez, J. F. Sierra, W. Savero Torres, A. Arrighi, F. Bonell, M. V. Costache, and S. O. Valenzuela,

Strongly anisotropic spin relaxation in graphene–transition metal dichalcogenide heterostructures at room temperature, Nat. Phys. **14**, 303 (2017).

[36]B. Liu, W. Niu, Y. Chen, X. Ruan, Z. Tang, X. Wang, W. Liu, L. He, Y. Li, J. Wu, S. Tang, J. Du, R. Zhang, and Y. Xu, Ultrafast Orbital-Oriented Control of Magnetization in Half-Metallic $La_{0.7}Sr_{0.3}MnO_3$ Films, Adv. Mater. **31**, 1806443 (2019).

[37]X. Zhou, C. Fang, W.-F. Tsai, and J. Hu, Theory of quasiparticle scattering in a two-dimensional system of helical Dirac fermions: Surface band structure of a three-dimensional topological insulator, Phys. Rev. B **80**, 245317 (2009).

[38]Y. L. Chen, J. G. Analytis, J.-H. Chu, Z. K. Liu, S.-K. Mo, X. L. Qi, H. J. Zhang, D. H. Lu, X. Dai, Z. Fang, S. C. Zhang, I. R. Fisher, Z. Hussain, and Z.-X. Shen, Experimental Realization of a Three-Dimensional Topological Insulator, Bi_2Te_3, Science **325**, 178 (2009).

[39]Z. Z. Du, C. M. Wang, H. Z. Lu, and X. C. Xie, Band Signatures for Strong Nonlinear Hall Effect in Bilayer WTe_2, Phys. Rev. Lett. **121**, 266601 (2018).

[40]L. Muechler, A. Alexandradinata, T. Neupert, and R. Car, Topological Nonsymmorphic Metals from Band Inversion, Phys. Rev. X **6**, 041069 (2016).

[41]Y. Chen, Y. Chen, J. Ning, L. Chen, W. Zhuang, L. He, R. Zhang, Y. Xu, and X. Wang, Observation of Shubnikov-de Haas Oscillations in Large-Scale Weyl Semimetal WTe_2 Films, Chin. Phys. Lett. **37**, 017104 (2020).

[42]Y. Chen, R. Liu, Y. Chen, X. Yuan, J. Ning, C. Zhang, L. Chen, P. Wang, L. He, R. Zhang, Y. Xu, and X. Wang, Large-Area Freestanding Weyl Semimetal WTe_2 Membranes, Chin. Phys. Lett. **38**, 017101 (2021).

[43]M. Gao, M. Zhang, W. Niu, Y. Chen, M. Gu, H. Wang, F. Song, P. Wang, S. Yan, F. Wang, X. Wang, X. Wang, Y. Xu, and R. Zhang, Tuning the transport behavior of centimeterscale WTe_2 ultrathin films fabricated by pulsed laser deposition, Appl. Phys. Lett. **111**, 031906 (2017).

[44]J. A. Gupta, R. Knobel, N. Samarth, and D. D. Awschalom, Ultrafast Manipulation of Electron Spin Coherence, Science **292**, 2458 (2001).

[45]X. D. Xu, W. Yao, D. Xiao, and T. F. Heinz, Spin and pseudospins in layered transition metal dichalcogenides, Nat. Phys. **10**, 343 (2014).

[46]C. D. Stanciu, F. Hansteen, A. V. Kimel, A. Kirilyuk, A. Tsukamoto, A. Itoh, and T. Rasing, All-optical magnetic recording with circularly polarized light, Phys. Rev. Lett. **99**, 047601 (2007).

[47]F. Ceballos and H. Zhao, Ultrafast Laser Spectroscopy of Two-Dimensional Materials Beyond Graphene, Adv. Funct. Mater. **27** (2017).

[48]S. Tang, C. Zhang, D. Wong, Z. Pedramrazi, H.-Z. Tsai, C. Jia, B. Moritz, M. Claassen, H. Ryu, S. Kahn, J. Jiang, H. Yan, M. Hashimoto, D. Lu, R. G. Moore, C.-C. Hwang, C. Hwang, Z. Hussain, Y. Chen, M. M. Ugeda, Z. Liu, X. Xie, T. P. Devereaux, M. F. Crommie, S.-K. Mo, and Z.-X. Shen, Quantum spin Hall state in monolayer 1T'-WTe_2, Nat. Phys. **13**, 683 (2017).

[49]J. Jiang, F. Tang, X. C. Pan, H. M. Liu, X. H. Niu, Y. X. Wang, D. F. Xu, H. F. Yang, B. P. Xie, F. Q. Song, P. Dudin, T. K. Kim, M. Hoesch, P. K. Das, I. Vobornik, X. G. Wan, and D. L. Feng, Signature of Strong Spin-Orbital Coupling in the Large Nonsaturating Magnetoresistance Material WTe_2, Phys. Rev. Lett. **115**, 166601 (2015).

[50]M. X. Guan, E. Wang, P. W. You, J. T. Sun, and S. Meng, Manipulating Weyl quasiparticles by orbital-selective photoexcitation in WTe_2, Nat. Commun. **12**, 1885 (2021).

[51]I. Pletikosic, M. N. Ali, A. V. Fedorov, R. J. Cava, and T. Valla, Electronic structure basis for the extraordinary magnetoresistance in WTe_2, Phys. Rev. Lett. **113**, 216601 (2014).

[52]R. J. Elliott, Theory of the Effect of Spin-Orbit Coupling on Magnetic Resonance in Some Semiconductors, Phys. Rev. **96**, 266 (1954).

[53]I. Zutic, Spintronics: Fundamentals and applications, Rev. Mod. Phys. **76**, 323 (2004).

[54]P. Boguslawski, Electron-electron spin-filp scattering and spin relaxation in III-V and II-VI semiconductors, Solid State Commun. **33**, 389 (1980).

Figure Captions

FIG. 1. (a) Schematic lattice structure of WTe_2 with side view (*bc* plane) and top view (*ab* plane). Tungsten atomic chains distort along the *b* direction (*ab* plane). (b) Schematic diagram of TR-MOKE setup. φ represents the rotation angle with respect to the incident plane of probe light. α is defined as the azimuthal angle between the crystallographic axis [100] of the WTe_2 film and the spatial *x* axis. $\lambda/2$: half-wave plate. $\lambda/4$: quarter-wave plate. (c) Time-resolved Kerr rotation traces under excitation of σ^+ and σ^- (pump light) along with the signals difference $[\Delta\theta_k(\sigma^+) - \Delta\theta_k(\sigma^-)]$ between σ^+ and σ^-.

FIG. 2. (a) The net Kerr signals as a function of delay time at the different φ. The dashed lines represent the ground states. (b) The net Kerr signal as a function of delay time at $\varphi = 10^o$ fitted by a biexponential decay model. (c) The φ dependence of fitted A_1, A_2 from the net Kerr signals. Here φ ranges from 0^o to 180^o. The red and black curves are the fitted lines by the double-sine function. (d) The φ dependent spin lifetimes (τ_1 and τ_2) deduced from the net Kerr signals. The average values of τ_1 and τ_2 are 0.8 ps and 5.9 ps, respectively.

FIG. 3. (a) The transient reflectivity spectrum fitted by the biexponential decay model. (b) The spin relaxation process of the WTe_2 films with the different defect density at $\varphi = 10^o$. The insets are the partial data around the origin.

FIG. 4. (a) The α dependence of fitted A_1 and A_2. α ranges from 0^o to 180^o. The red and black curves are the guide lines of six-fold symmetrical sine function. (b) Diagrammatic sketch of the Fermi surface map of one domain. The purple (yellow) rectangle shows the detected area of P-pol (S-pol) probe beam according to the matrix element effect. (c) Schematic diagram of WTe_2 energy band structure with the ultrafast spin relaxation process. The horizontal dashed line shows the position of the Fermi level (E_F). Green solid circles represent the excited electrons. The dotted rectangular box shows the enlarged region around the E_F, in which the red (blue) curve represents the energy band with spin up (down).

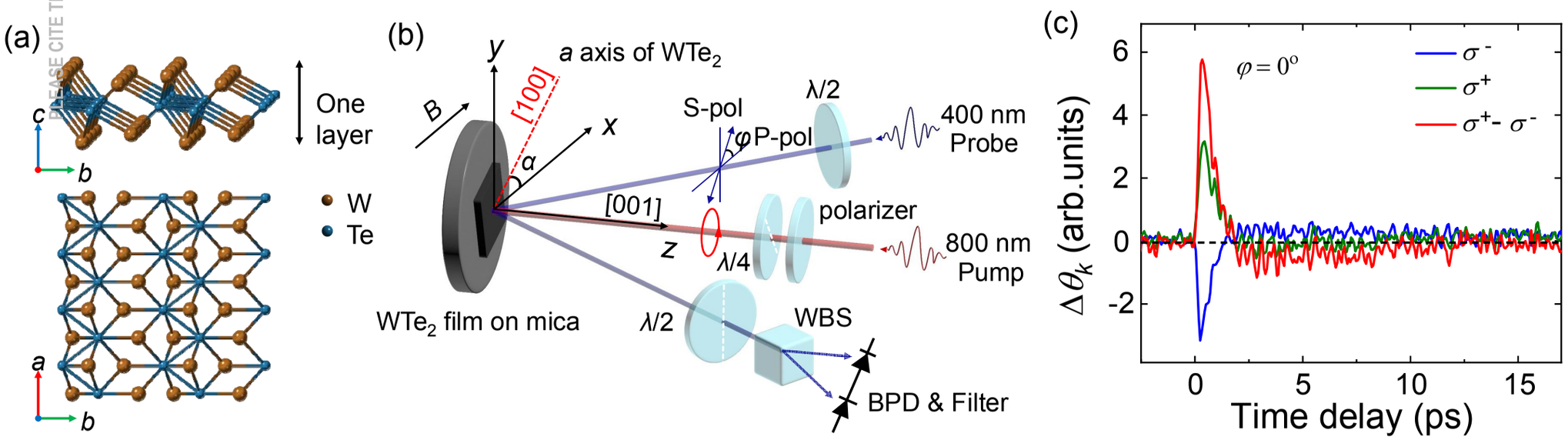

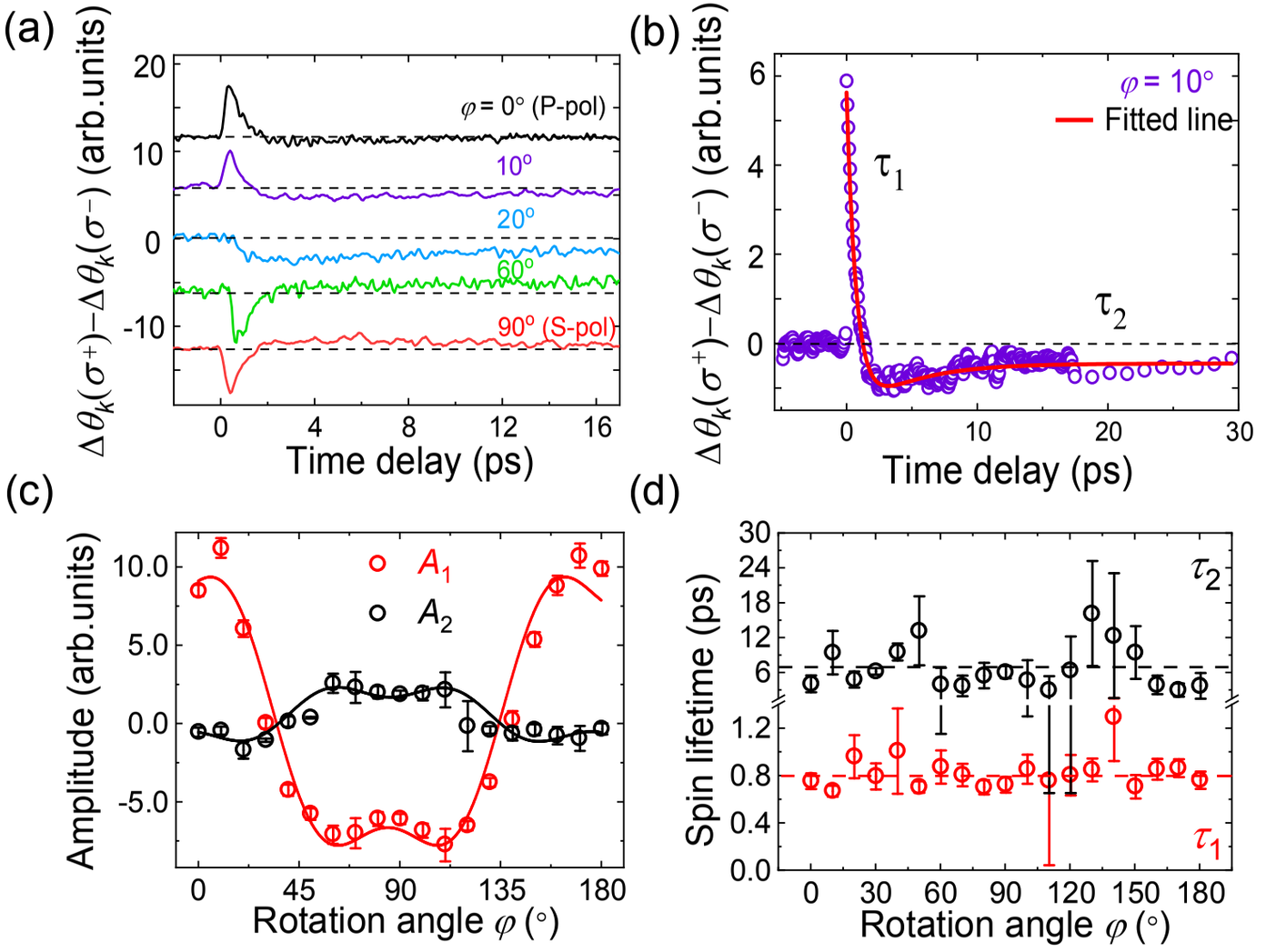

PLEASE CITE THIS ARTICLE AS DOI: 10.1063/5.0090935